



Integrative modeling of caprock integrity in the context of CO₂ storage: evolution of transport and geochemical properties and impact on performance and safety assessment

Bildstein O.¹, Kervévan C.², Lagneau V.³, Delaplace P.⁴, Crédoz A.¹, Audigane P.², Perfetti E.⁴, Jullien M.¹

¹CEA, DEN, DTN, Cadarache, 13108 Saint Paul lez Durance, France

²BRGM, Service Eau, 45060 Orléans Cedex 2, France

³Mines ParisTech, Centre de Géosciences, 77305 Fontainebleau Cedex, France

⁴IFP, Division Ingénierie de Réservoir, 92852 Rueil-Malmaison, France

1. ABSTRACT

The objective of the “Géocarbone-Intégrité” project (2005-2008) was to develop a methodology to assess the integrity of the caprock involved in the geological storage of CO₂. A specific work package of the project (WP5) was dedicated to the integration of (1) the phenomenology describing the evolution of the storage system with a focus on the mechanisms occurring in the caprock and at the interface with the caprock, and (2) the data obtained from the investigation of petrographical, geomechanical, and geochemical properties, before and after reaction with CO₂-rich solutions, performed in the other work packages (WP1 to WP4). This knowledge was introduced in numerical models and specific safety scenarios were defined in order to assess the performance of the CO₂ storage system.

The results of the modeling show that the injection of CO₂ can potentially have a significant effect on the caprock by changing the porosity due to the dissolution and precipitation of minerals, but that the impact is limited to a zone from several decimeters to several meters of the caprock close to the interface with the reservoir depending on whether the supercritical carbon dioxide (SC-CO₂) plume enters into the caprock and if fractures are present at this location.

The methodology used in this project can be applied to a pilot site for the injection of CO₂ in the Paris Basin. A key aspect of the safety of such a facility will be to look at the coupling of geochemical alteration and the evolution of geomechanical properties in the short and medium terms (several hundreds of years). The challenge for the future will be to structure and apply the safety assessment methodology with an operational finality, in order to support the robustness of the transition step to CGS projects at the industrial scale.

2. RESUME

Le Volet 5 du projet « Géocarbone-Intégrité » visait à intégrer l'ensemble des mécanismes étudiés dans les quatre premiers volets du projet pour une évaluation de performance des couvertures et une étude de sûreté afin de s'assurer de leur préservation et de leur intégrité sur le long terme (de l'ordre du millénaire). L'objectif est d'une part d'aboutir à la construction d'un modèle phénoménologique multi-échelle global, puis à un modèle numérique décrivant le confinement du CO₂ par les couvertures et, d'autre part, de déterminer les performances du confinement en identifiant les processus clefs et les paramètres les plus influents.

Une première partie du programme a consisté en une intégration spatiale de l'ensemble des données phénoménologiques et structurales disponibles à la suite des travaux réalisés dans les différents volets (WP1 à WP4) et à la définition des scénarios types d'évolution du site de stockage (niveaux réservoirs et encaissants). Ce travail a permis de définir les cas tests à

49 prendre en compte et de réaliser les calculs de performance par rapport aux scénarios
50 d'injection et par rapport aux hétérogénéités majeures identifiées dans les niveaux de
51 confinement (notamment les fractures).

52 Les résultats montrent que l'injection de CO₂ peut avoir un effet significatif, en
53 altérant la porosité par dissolution et précipitation de minéraux, mais que l'impact est limité
54 dans l'espace, de quelques décimètres à quelques mètres de l'interface réservoir-couverture,
55 selon que la bulle de CO₂ supercritique pénètre ou non dans la couverture et selon la présence
56 ou l'absence de fractures.

57 La prise en compte des résultats issus de l'analyse de sensibilité et l'analyse des
58 incertitudes permettra de conduire des calculs de sûreté plus précis. Appliqués au futur site
59 d'injection, ces calculs permettront d'évaluer la pérennité des propriétés de confinement des
60 couvertures et de valider la qualité de confinement du site de stockage de CO₂. Il conviendra
61 notamment d'évaluer l'impact du couplage entre les phénomènes géochimiques et
62 géomécaniques sur le court et moyen terme (de l'ordre de la centaine d'année). Le défi pour
63 l'avenir est de structurer et d'appliquer la méthodologie de l'analyse de sûreté, en mettant en
64 avant la finalité opérationnelle, de manière à assurer la robustesse de la transition vers les
65 projets de CGS à l'échelle industrielle.
66

67 3. INTRODUCTION

68
69 The storage of CO₂ in deep saline aquifers and depleted oil and gas reservoirs for
70 periods of time of ~1,000-10,000 years is considered in order to mitigate its release in the
71 atmosphere and avoid the consequences of the additional greenhouse effect on climate change
72 (IPCC, 2005). The feasibility of such an industrial process and the safety on the long term has
73 to be demonstrated and relies mainly on the confinement properties of the caprock. In general,
74 the knowledge of the structure, the properties and the reactivity of the caprock is poor because,
75 usually, the reservoir is the main object of interest for oil and gas production.

76 The objective of the "Geocarbone-Intégrité" project (2005-2008) was therefore to
77 develop a methodology and to design a tool to assess the integrity of the caprock involved in
78 the geological storage of CO₂. A specific work package of the project (WP5) was dedicated to
79 the integration of (1) the phenomenology describing the evolution of the storage system with
80 a focus on the mechanisms occurring in the caprock and at the interface with the caprock, and
81 (2) the data obtained from the investigation of petrographical, geomechanical, and
82 geochemical properties, before and after reaction with CO₂-rich solutions, performed in the
83 other work packages (WP1 to WP4) (see Fleury et al., *this issue*, for a detailed description of
84 the project). The ultimate goal is to construct a conceptual and numerical model at the site
85 scale to predict the evolution of the storage on the long term and to ensure the persistence of
86 the caprock integrity. This model is developed in the perspective of the assessment of the
87 performance and safety of the future injection pilot site in the Paris Basin planned to be
88 commissioned in 2010.

89 A review of the existing literature on CO₂ storage modeling reveals that most of the
90 effort made by the scientific community are devoted to the study of injectivity properties and
91 mineral trapping capability in reservoirs (see review by Gaus et al., 2008). The studies on
92 caprock integrity are still relatively rare, and only recently some insights on caprock
93 mineralogical alteration patterns induced by CO₂ migration have been gained by means of
94 reactive transport modeling techniques (Johnson et al., 2004, 2005; Gauss et al., 2005; Xu et
95 al., 2005; Gherardi et al. 2007). This study is focused on the numerical prediction of the long
96 term variations of the mineralogical and hydraulic properties of the caprock in the French
97 pilot site for CO₂ geological storage, in the Paris Basin.

100 4. PHENOMENOLOGY OF THE STORAGE

101

102 4.1. Physicochemical processes at the interface with the caprock

103

104 The phenomenology of the storage is described in detail in a special report of the
105 Intergovernmental Panel on Climate Change dedicated to the capture and storage of CO₂
106 (IPCC, 2005). The injected CO₂ is usually at supercritical conditions (SC-CO₂) in the typical
107 reservoir pressure and temperature conditions (63°C and 145 bar in the case of the Saint
108 Martin-de-Bossenay field - Paris basin, France). Under these conditions, the fluid properties
109 of SC-CO₂ are similar to both a liquid phase (density around 0.6) and a gas phase (low
110 viscosity; e.g. Mathias et al. 2009). Also, CO₂ is very soluble in water: about 1 mol/l (e.g.,
111 Duan and Sun, 2003). Its migration in porous media (reservoirs and caprocks) containing
112 water involves capillary effects.

113 Since SC-CO₂ is less dense than water, it will rise in the reservoir. A fraction of this
114 CO₂ will be trapped in the porosity (capillary trapping) and the rest will reach the structural
115 trap (or stratigraphical trap) constituted by the caprock, which is expected to prevent the CO₂
116 from rising any further and eventually reaching the atmosphere. This is due to the properties
117 of the caprock which is usually a clay-rich material, saturated with water and characterized by
118 a very low permeability and a high gas entry pressure. The caprock will therefore be in
119 physical contact with the SC-CO₂ plume during most of the storage lifetime.

120 If the overpressure of SC-CO₂ is lower than the capillary entry pressure, the SC-CO₂
121 will remain confined in the reservoir. However, dissolved CO₂ will still be able to diffuse into
122 the caprock. This is a slow transport process but the dissolution of CO₂ can strongly affect the
123 composition of the formation water, in particular, by lowering the local pH. This change can
124 potentially damage the caprock by destabilizing the chemical equilibrium with the primary
125 mineral phases and triggering the dissolution of some of them and the precipitation of
126 secondary phases.

127 If the overpressure at the interface between the reservoir and the caprock overcomes the
128 entry pressure, the SC-CO₂ will penetrate into the caprock, due to the pressure gradient and
129 the buoyancy forces, and will displace the caprock water. If the pressure further builds up, the
130 plume can potentially force its way, in mechanical terms, into the caprock through dilatancy
131 driven flow or induced fracturing.

132

133 Importantly, any heterogeneity in the caprock, such as small cracks or fractures, will
134 facilitate the migration of SC-CO₂ into the caprock. The behavior of these preferential
135 pathways and the reactivity with the CO₂-rich fluids is critical for the understanding of the
136 evolution of the confinement properties of the caprock. To this regard, the dissolution of the
137 mineral phase constituting the cement of the rock (e.g. carbonates) can potentially open or
138 close the porosity and affect the permeability of the matrix as well as of the cracks and
139 fractures. The same effect can be obtained by altering potentially expansive primary clay
140 minerals and forming secondary non-swelling ones (e.g. through the illitization process;
141 Crédoz *et al.*, 2009).

142 A last potentially important migration pathway for CO₂, which was not investigated in
143 this work, is the possibility of having defective abandoned wells present in the zone
144 influenced by the injection.

145

146

147 4.2. Scenarios for the evolution of the storage

148 The following scenarios have been considered to predict the fate of SC-CO₂ at the
149 interface between reservoir and caprock (Figure 1):

- 150 1. The SC-CO₂ overpressure at the top of the reservoir is **lower than the**
151 **capillary entry pressure in the caprock**. As a consequence, the SC-CO₂
152 cannot penetrate into the caprock but dissolved CO₂ and acidified formation
153 water can penetrate into the caprock by diffusion, triggering geochemical
154 alteration. This is the *reference case scenario* for the safety assessment
155 (section 5.2.1, *case 1a*, *case 1b*, and *case 1c*).
- 156 2. The SC-CO₂ does not directly enter into the rock matrix but penetrates the
157 caprock through a network of connected fractures. This is the "*fracture*
158 *network*" *scenario* which is considered as probable and constitutes a first
159 altered scenario for the safety assessment. Only a dissolved CO₂ is considered
160 in this fracture scenario (section 5.2.2, *case 2*).
- 161 3. The SC-CO₂ overpressure at the reservoir top is **higher than the capillary**
162 **entry pressure in the caprock**. In this case, the SC-CO₂ enters into the
163 caprock by forced drainage. This is the *multiphase scenario* where the SC-
164 CO₂ migration is controlled by the effective caprock permeability. This
165 scenario is considered as highly probable in the injection phase (due to
166 significant overpressure) and constitutes a second altered scenario for the
167 safety assessment (section 5.3, *case 3*).

168

169 The chosen scenarios mainly focus on the geochemical effects induced by the
170 advancement of both a CO₂-rich aqueous phase and a free SC-CO₂ gas plume through the
171 caprock. A fractured caprock scenario is also simulated but the focus is concentrated on
172 geochemical reactions with the filling material (calcite). In this work, worst case scenarios
173 based on "hydrodynamic" leaking of CO₂, e.g. through open fractures, are not investigated
174 and therefore the results presented here does not constitute a full safety assessment exercise.

175

176 The effect of gas-rock interactions has not been considered in our calculations because
177 most of the reactivity is expected to occur at the interface between rock and aqueous phase.
178 This is supported by the fact that high residual water contents (liquid saturation, S_L , always
179 greater than about 0.6) have been calculated even for the case of most significant penetration
180 of SC-CO₂ into the caprock.

181

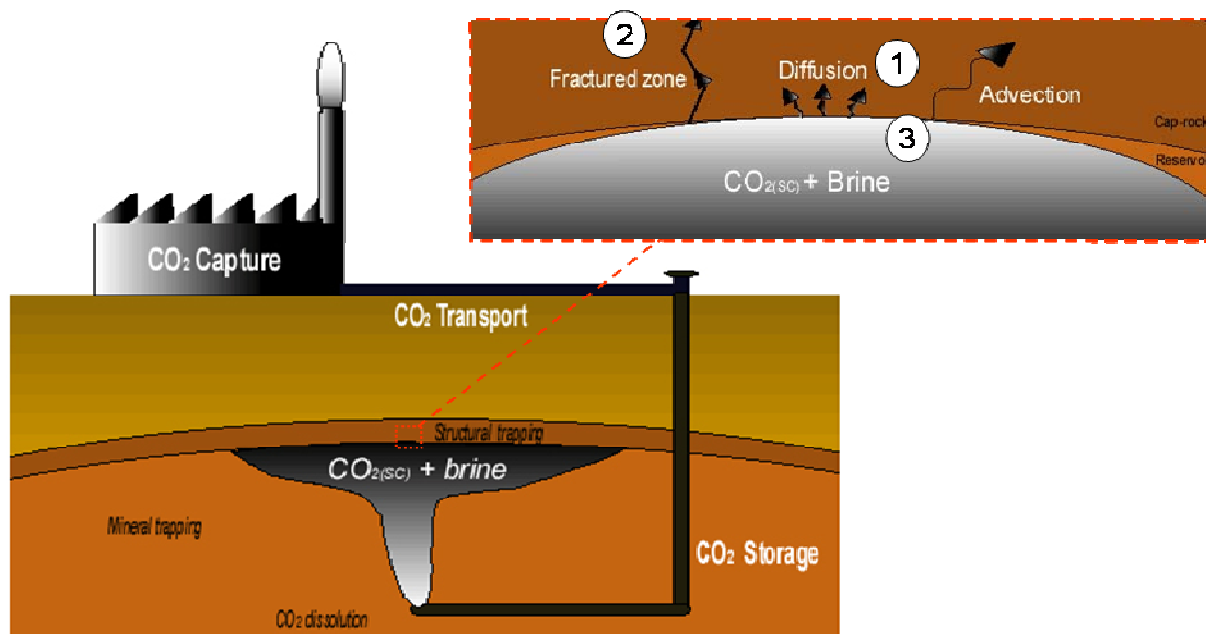


Figure 1. Scenarios for the evolution of the reservoir/caprock system during CO₂ injection.

5. ASSESSMENT OF CAPROCK INTEGRITY PERSISTENCE WITH TIME

The impact of geochemical alteration of the caprock, in terms of confinement properties, on transport properties such as permeability depends primarily on the initial value of these parameters and on the net volume balance of mineral reactions, i.e. dissolution and precipitation (Bemer and Lombard, 2009).

The geochemical reactivity of the caprock and its constitutive minerals has been investigated in WP4 of the “Géocarbonate-Intégrité” project which aimed at determining the reaction pathways for SC-CO₂/water/rock interactions and also kinetic parameters for carbonate and clay mineral transformations (Kohler and Parra, 2007; Crédoz *et al.*, 2009; Hubert, 2009).

These parameters have to be integrated into large scale modeling in order to calculate the evolution of the storage system as a result of the CO₂ perturbation. A major challenge of this type of modeling is to extrapolate the behavior of the system from the lab scale to the field scale, including:

- time: 1 year for experiments vs. 10,000 years for geological storage,
- solid/solution ratio: around 50 g/L in experiments vs. about 50 kg/L in depth,
- texture: fine crushed rock (0.1 mm particles) vs. bulk rock,
- temperature: 80-150°C in the experiments vs. 65°C in Saint Martin-de-Bossenay (Paris Basin, France).

In the laboratory, the conditions are chosen so that the reactivity of the samples is enhanced in order to limit the duration of the experiments. For the large scale calculations, it is crucial to set these parameters to realistic values but the effect of the texture is difficult to determine except through values of the reactive surface area. Petrophysical and geochemical parameters are given for the different scenarios considered in Table 1 which are used for 1D and 2D calculations with a simplified caprock geometry (15% porosity, 1 to 10 meters thick).

5.1. Modeling approach

At the beginning of the project, the collaborative work between different modeling teams was organized much in the same way as the IPCC modeling of climate (IPCC, 2007), i.e. defining a set of common guidelines and parameters for the modeling (Table 1) but also giving some degree of liberty concerning the way to carry out the calculations, in particular:

- the choice of the numerical tool,
- the capillary and permeability properties,
- the list of secondary minerals allowed to precipitate, and to some extent of primary minerals as well,
- the values for the mineral kinetic constants for precipitation and dissolution and the reactive surface area,
- the feedback between mineral dissolution/precipitation and the transport parameters (diffusion coefficient, permeability, capillary curve, ...)

In this way, the modeling exercise should not be considered as a benchmarking of different modeling tools but rather as an investigation of the dominant processes and the most influential parameters giving an envelope of behaviors for the storage system. Only one representative set of results is shown for a specific scenario if all the modeling teams involved in the calculations reached the same conclusions. If the conclusion is significantly different, a comparison and analysis of the results is presented.

Guidelines for the modeling scenarios

A first series of calculations in scenarios where the porous media are saturated (Table 1: cases 1a to 1c and case 2, respectively corresponding to scenarios 1 and 2) were performed with reactive transport tools available in the different modeling teams: Crunch (Steeffel, 2001), Hytec (van der Lee et al., 2003), PhreeqC (Parkhurst and Appelo, 1999), PHAST (Parkhurst et al. 2004). The thermodynamic database used for the calculations is derived from EQ3/6 code (Wolery, 1992), and the kinetic data for the dissolution (and to a lesser degree for the precipitation) of mineral phases were taken from the review by Palandri and Kharaka (2004).

A second series of calculations using the same scenarios involved multiphase flow and reactive transport in porous media (Table 1: case 3 corresponding to scenario 3) and were performed with TOUGHREACT (Xu and Pruess, 2001) and COORESTM (e.g. Le Gallo et al. 2007).

Reference case		Sensitivity analysis
Duration = 10000 years - Temperature = 80°C		
Caprock initial composition	based on Charmotte/Saint Martin-de-Bossenay (Paris basin)	
Water initial composition	in equilibrium with caprock mineralogy (pH = 6.5)	
Boundary condition (constant concentration)	(1a) acidified water starting from Dogger formation $\text{CO}_2(\text{aq}) = 1.1$ molal in equilibrium with $\text{pCO}_2 = 150$ bar (pH = 4.7) (1b) initial composition acidified with $\text{pCO}_2 = 150$ bar and buffered with carbonates (pH = 4.6) (1c) initial composition acidified with $\text{pCO}_2 = 150$ bar (pH = 3.4)	(1a) water from Dogger formation (pH = 6.2) (1b) initial composition acidified with $\text{pCO}_2 = 150$ bar (pH = 3.4)
1) 1D Diffusive/convection case (1a, 1b, 1c)		

Porosity	15%	(1a) 5%
Effective diffusion coefficient	10^{-11} m ² /s	(1a) 10^{-10} m ² /s
Permeability	(1c) $K = 1.6 \cdot 10^{-18}$ m ²	
Flow rate	10x diffusive flux	
2) 2D system with discrete fracture (case 2)		
Mineralogy and water composition	based on case 1c	
Fracture filled with calcite	porosity 40%	
Fracture permeability	10,000 x higher than in reservoir (case 1c)	
3) 1D multiphase case (case 3)		
Mineralogy and water composition	based on single-phase case 1a	
Boundary condition	constant pressure	
Relative permeability	Van Genuchten model (see Eq. 1 and 2) $K = 10^{-18}$ m ²	
Capillary pressure	Van Genuchten model (see Eq. 3)	
Effective diffusion coefficient	10^{-11} m ² /s	

249 **Table 1. Modeling parameters for the reference case simulation and sensitivity analyses.**

250
251 Note that for the boundary conditions, the chemical composition of reservoir pore waters
252 remain fixed during the simulation. For the cases with acidified waters, it means that the pH
253 in the reservoir is controlled by the CO₂-plume during 10,000 years, even though control
254 should be taken over by the reservoir water composition again at some point after the end of
255 the CO₂ injection. It is however considered here as a conservative assumption for the
256 performance and safety of the storage.
257

258 **5.2. Saturated caprock: geochemical interactions with dissolved CO₂**

259
260 In these scenarios, the SC-CO₂ plume is trapped in the reservoir and the acidic
261 perturbation migrates by diffusion of dissolved species only.

262 **5.2.1. Homogeneous caprock, diffusive/advective case**

263
264 In these calculations, the diffusion coefficient is set initially to 10^{-11} m²/s, which is the
265 mean value measured in the argillites from Bure (Talandier et al., 2006) and considered as
266 analogues to the clay series in the caprock investigated in the framework of this project. More
267 details about diffusion coefficients can be found in Fleury et al. (2009) and Berne et al. (2009).
268 Some sensitivity calculations are also shown which investigate the influence of this parameter.
269

270 ***Case 1a: pure diffusion, specific water compositions for the reservoir and caprock***

271 In this case, the caprock is initially homogeneous in composition (mineralogy and pore
272 water) and in transport properties (no cracks or fractures or other preferential pathways).
273 Preliminary batch calculations were conducted in order to determine possible secondary
274 mineral phases that potentially precipitate in this context. Some simplifications were made in
275 the calculations in order to avoid dealing with complex solid-solutions: clay minerals are
276 represented only by pure end-members (it concerns especially the interstratified illite-smectite
277 minerals), mixed carbonates such as ankerite are considered with a constant composition
278 (Table 3). In this series of simulations, the acidified water ($pCO_2 = 150$ bar) used as the
279 boundary condition at the contact with the caprock is equilibrated with the mineral
280 assemblage of the reservoir. Under this hypothesis, the water can be considered as less

281 aggressive with respect to the caprock minerals than in the configuration where the water is
 282 only acidified by CO₂ (*case Ib*). The water compositions considered here, based upon data
 283 from Azaroual et al. (1997), are detailed in Table 2.

284 A 1D geometry was considered within the caprock assuming an initial equilibrium
 285 between the water (Table 2, 3rd column) and the mineral phases constituting the caprock
 286 (Table 3). The base of the modeled domain was supposed to be permanently in contact with
 287 the acidified reservoir water (Table 2, 2nd column) so that dissolved CO₂ is transported by
 288 molecular diffusion within the caprock.

289 We performed several simulations considering various typical initial porosities (15 and
 290 5%) and diffusion coefficient values (10⁻¹¹ and 10⁻¹⁰ m².s⁻¹). The codes PHREEQC and
 291 PHAST were used with various meshes (about 100 grid cells, with both uniform and variable
 292 grid spacing) and time-stepping in order to increase the robustness of the calculations
 293 presented hereafter (Figure 2 and Figure 3).

294
 295

Reference Dogger reservoir water (80°C)*		Acidified reservoir water (80°C, pCO ₂ = 150 bar)*		Initial caprock water (80°C)	
pH	6.24	pH	4.75	pH	6.54
Species	Molality	Species	Molality	Species	Molality
Al	5.622 10 ⁻⁸	Al	1.251 10 ⁻⁷	Al	1.531 10 ⁻⁷
C	4.895 10 ⁻³	C	1.141	C	2.180 10 ⁻³
Ca	1.612 10 ⁻²	Ca	3.204 10 ⁻²	Ca	1.528 10 ⁻²
Cl	3.014 10 ⁻¹	Cl	3.015 10 ⁻¹	Cl	2.601 10 ⁻¹
Fe	2.137 10 ⁻⁷	Fe	1.751 10 ⁻⁶	Fe	1.534 10 ⁻⁵
K	2.374 10 ⁻³	K	2.375 10 ⁻³	K	1.190 10 ⁻²
Mg	1.282 10 ⁻²	Mg	2.424 10 ⁻²	Mg	8.937 10 ⁻⁴
Na	2.594 10 ⁻¹	Na	2.595 10 ⁻¹	Na	2.543 10 ⁻¹
S	7.642 10 ⁻³	S	7.649 10 ⁻³	S	1.841 10 ⁻²
Si	8.994 10 ⁻⁴	Si	8.833 10 ⁻⁴	Si	5.371 10 ⁻⁴

(*) equilibrated with the assumed reservoir mineralogy (calcite, dolomite-dis, chalcedony, illite, pyrite)

296
 297

298 **Table 2. Water compositions considered in the simulations.**

299

Mineral phase	Initial weight %	log(K) at 80°C	reaction	SI(1)	SI(2)	SI(3)
Calcite	50	1.05	Calcite + H ⁺ = Ca ⁺⁺ + HCO ₃ ⁻	0	0	0
Ankerite	5	12.14	Ankerite + 4H ⁺ = Ca ⁺⁺ + 0.3Mg ⁺⁺ + 0.7Fe ⁺⁺ + 2H ₂ O + 2CO _{2(aq)}	-0.99	-0.99	0
Montmorillonite-Na	25	-0.65	Mont-Na + 6H ⁺ = 0.33 Mg ⁺⁺ + 0.33 Na ⁺ + 1.67Al ⁺⁺⁺ + 4H ₂ O + 4SiO _{2(aq)}	0.77	0.52	0
Kaolinite	3	2.38	Kaolinite + 6H ⁺ = 2Al ⁺⁺⁺ + 2SiO _{2(aq)} + 5H ₂ O	0.13	1.49	0
Illite	2	3.80	Illite + 8H ⁺ = 0.25Mg ⁺⁺ + 0.6K ⁺ + 2.3Al ⁺⁺⁺ + 3.5SiO _{2(aq)} + 5H ₂ O	0	0	0
Quartz	10	-3.24	Quartz = SiO _{2(aq)}	0.23	0.23	0
Anhydrite	3	-5.05	Anhydrite = Ca ⁺⁺ + SO ₄ ⁻⁻	-0.47	-0.34	0
Pyrite	2	-21.91	Pyrite + H ₂ O = 0.25H ⁺ + 0.25SO ₄ ⁻ + Fe ⁺⁺ + 1.75HS ⁻	0	0	0
<i>Goethite</i>	-	-1.13	Goethite + 3H ⁺ = Fe ⁺⁺⁺ + 2H ₂ O	-2.65	-5.20	6e-4
<i>Chalcedony</i>	-	-3.02	Chalcedony = SiO _{2(aq)}	0	0	-0.23
<i>Disordered-Dolomite</i>	-	1.92	Dolom-dis + 2H ⁺ = Ca ⁺⁺ + Mg ⁺⁺ + 2HCO ₃ ⁻	0	0	-1.24
<i>Siderite</i>	-	-1.17	Siderite + H ⁺ = Fe ⁺⁺ + HCO ₃ ⁻	-2.78	-2.78	-0.84

300 **Table 3. Initial mineral composition of the caprock (inspired from the Charmotte field) and**
 301 **secondary phases (*in italics*) taken into account in the model. Equilibrium constants at 80°C and**
 302 **reactions are given for each mineral. SI(1), SI(2), and SI(3) refer to the initial saturation indexes**
 303 **of the mineral phases in the Dogger, acidified, and caprock waters respectively.**

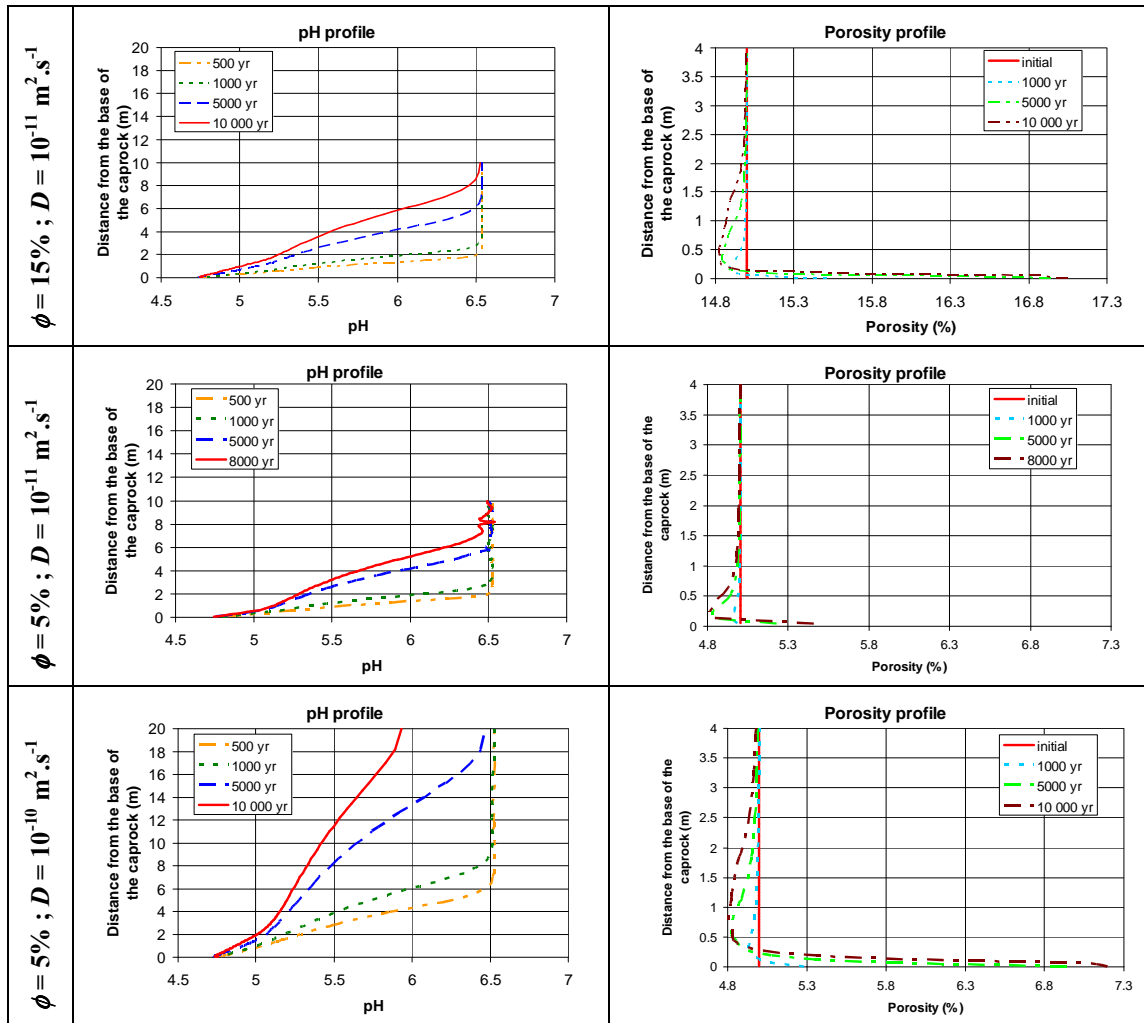
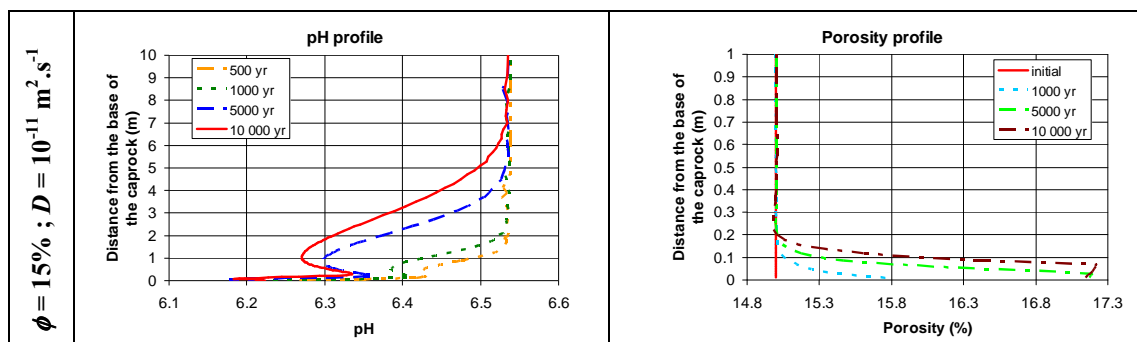


Figure 2. Diffusion of the acidified reservoir water: pH and porosity profiles in the caprock calculated for several porosity (15 and 5%) and diffusion coefficient (10^{-11} and $10^{-10} \text{ m}^2 \cdot \text{s}^{-1}$) values. (Note zoom over 4 m in porosity profiles)

305
306
307
308
309
310
311
312
313
314
315
316
317
318
319
320
321

In all cases, similar trends and orders of magnitude for pH and porosity profiles along the first few meters of the caprock are observed after a simulation period up to ten thousands years (Figure 2). As expected, the acidified water penetrates the caprock on a distance increasing with the diffusion coefficient value (see pH profiles). However, the impact on the minerals remains comparable (mainly: dissolution of illite and anhydrite, precipitation of calcite, montmorillonite-Na and kaolinite), showing no significant sensitivity towards initial porosity and diffusion coefficient values, as illustrated by the porosity profiles which integrate the volumetric variations of all the primary and secondary mineral phases considered in the chemical reactions (see Table 3). In all cases, both the amplitude and the extension of the variations observed along the modeled profile remain relatively limited: a first increase in porosity (up to +2.2%) within the first decimeters of the caprock domain is observed, followed by a slight decrease of the porosity value (around -0.2%) in the next 1 to 3 meters.



322 **Figure 3. Diffusion of the non-acidified reservoir water: pH and porosity profiles in the caprock**
 323 **calculated for a porosity of 15% and a diffusion coefficient of $10^{-11} \text{ m}^2 \cdot \text{s}^{-1}$.**

324
 325 Note that the water compositions described in Table 2 also show a significant contrast
 326 between the initial caprock water and the original reservoir water. Formation water indeed
 327 often show differences which are not completely balanced by diffusion at the interface.
 328 Interdiffusion processes can potentially induce some transformations in the mineral
 329 composition at this location. In order to quantify this effect and discriminate the role of
 330 dissolved CO_2 , we performed another simulation for the first parameter set ($\phi = 15\%$;
 331 $D = 10^{-11} \text{ m}^2 \cdot \text{s}^{-1}$) now using columns 1 and 3 in Table 2 as boundary and initial water
 332 compositions, respectively. The results obtained are presented in Figure 3. As expected, pH
 333 variations along the profile are much smaller in amplitude than in the “acidified water” case
 334 (ranging here between 6.2 and 6.5). The behavior of the system, in terms of mineral reactivity,
 335 is comparable to the previous simulations with acidified water (*i.e.*, dissolution of illite and
 336 anhydrite, precipitation of calcite, montmorillonite-Na and kaolinite) but remains limited to
 337 the very first decimeters of the caprock. However, the impact on porosity is significant as
 338 shown by the porosity profiles in Figure 3. When compared to the profiles in Figure 2, it can
 339 be noticed that the amplitude of the increase in porosity (varying from 15 to 17%) is quite
 340 similar. In this case, however, no decrease of the porosity is observed in the first meter of the
 341 caprock.

342
 343 The results obtained in this last simulation give us some new insight into the specific role of
 344 the initial water composition and the pH perturbation due to CO_2 . The distinct impact of the
 345 initial water was also observed in experiments where the caprock from the Paris Basin was
 346 reacted with typical reservoir water from the Dogger formation (Crédoz et al., 2009).

348 **Case 1b: pure diffusion, same initial water composition in reservoir and caprock**

349 The mineral composition corresponds to that of the transition zone between the
 350 reservoir and the caprock in the Charmotte area (Paris Basin, France) (Table 4). The initial
 351 water composition is in equilibrium with the mineral assemblage of the caprock. Two water
 352 compositions are considered at the boundary (*i.e.* at the interface between the caprock and the
 353 reservoir). In both case, the water is similar to the previous one, except for the acidification of
 354 the water due to the dissolution of CO_2 in the reservoir (Table 5). For the first one, we
 355 consider the acidification effect but also some short term buffering capacity of minerals
 356 (essentially carbonates and sulfates) which reacted with the CO_2 plume and the solution
 357 during the migration of the plume in the reservoir. This case resembles the previous *case 1a*
 358 (pH = 4.63). For the second one, we consider that the acidification is maximized (pH = 3.36,
 359 in equilibrium with CO_2 -SC only) in order to obtain the strongest pH perturbation possible in
 360 this system, *i.e.* testing extremely adverse conditions for safety assessment purposes. This
 361 scenario corresponds to a hypothetical case in which the minerals from the reservoir do not

362 buffer the pH (i.e., the residence time of the interstitial water is much shorter than the reaction
 363 kinetics characteristic time).
 364
 365

	Volume % (fraction of total rock volume)	Weight % (of solid)
<i>Porosity</i>	15	-
Clay fraction		
Illite	11	13
Montmor-Ca	2	3
Kaolinite	9	10
Silt fraction		
Quartz	9	10
Carbonate fraction		
Calcite	41	45
Dolomite	2	3
Siderite	1	2
Accessory minerals		
Pyrite	2	4
Anhydrite/gypsum	4	5
Anatase, other ...*	4	5

* considered as inert minerals

366
 367 **Table 4. Simplified composition used for calculations with the transition zone between reservoir**
 368 **and caprock at Charmotte (porosity = 15%).**

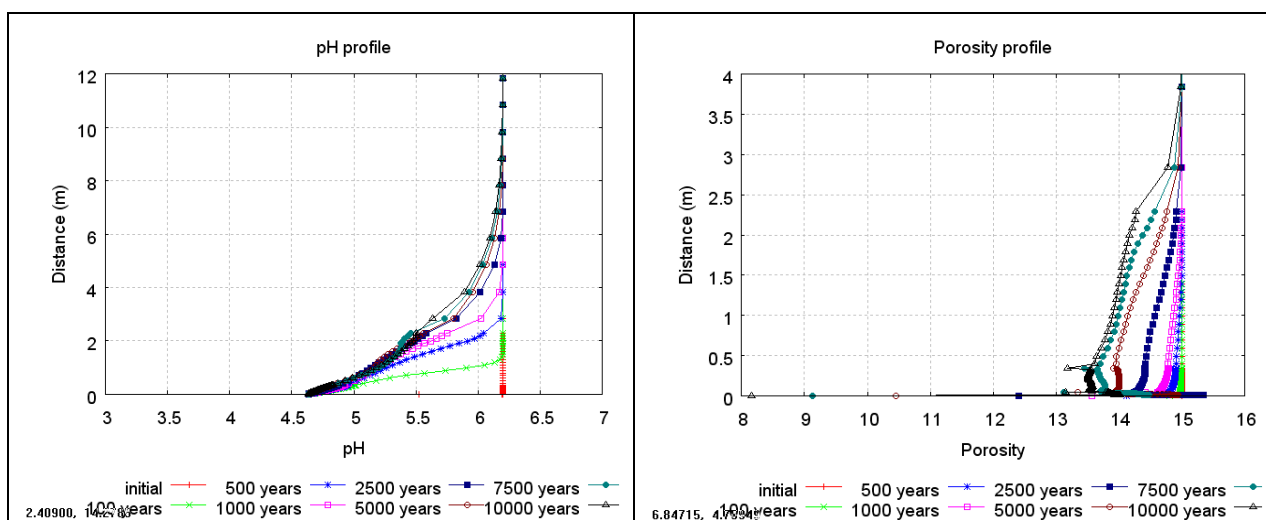
Charmotte transition zone water composition (80°C)*		Acidified water (80°C, pCO ₂ = 150 bar, fCO ₂ = 83 bar)		Acidified water equilibrated with carbonates* (80°C)	
pH	6.20	pH	3.36	pH	4.63
Species	Molality	Species	Molality	Species	Molality
Al	2.18 10 ⁻⁸	Al	2.18 10 ⁻⁸	Al	1.21 10 ⁻⁸
C	2.00 10 ⁻³	C	1.00	C	1.02
Ca	4.22 10 ⁻²	Ca	4.22 10 ⁻²	Ca	5.50 10 ⁻²
Cl	1.92 10 ⁻¹	Cl	1.92 10 ⁻¹	Cl	1.92 10 ⁻¹
Fe	1.22 10 ⁻⁵	Fe	1.22 10 ⁻⁵	Fe	9.30 10 ⁻⁶
K	1.85 10 ⁻²	K	1.85 10 ⁻²	K	1.85 10 ⁻²
Mg	1.12 10 ⁻²	Mg	1.12 10 ⁻²	Mg	1.52 10 ⁻²
Na	8.00 10 ⁻²	Na	8.00 10 ⁻²	Na	8.00 10 ⁻²
S	6.16 10 ⁻³	S	6.16 10 ⁻³	S	5.86 10 ⁻³
Si	6.55 10 ⁻⁴	Si	6.55 10 ⁻⁴	Si	2.48 10 ⁻⁴

* equilibrated with fast reacting minerals assumed to be present in reservoir (calcite, dolomite, anhydrite)

371
 372
 373 **Table 5. Water compositions considered in the simulations.**

374
 375 The calculations concerning the scenario with the pH 4.6 water entering the caprock
 376 shows that the alteration of the caprock is significant with a similar front of pH perturbation
 377 compared to *case Ia*, but the porosity change is very limited (Figure 4). The precipitation of
 378 anhydrite (+16%), kaolinite (+12%) and quartz (+2%) is responsible for the porosity decrease

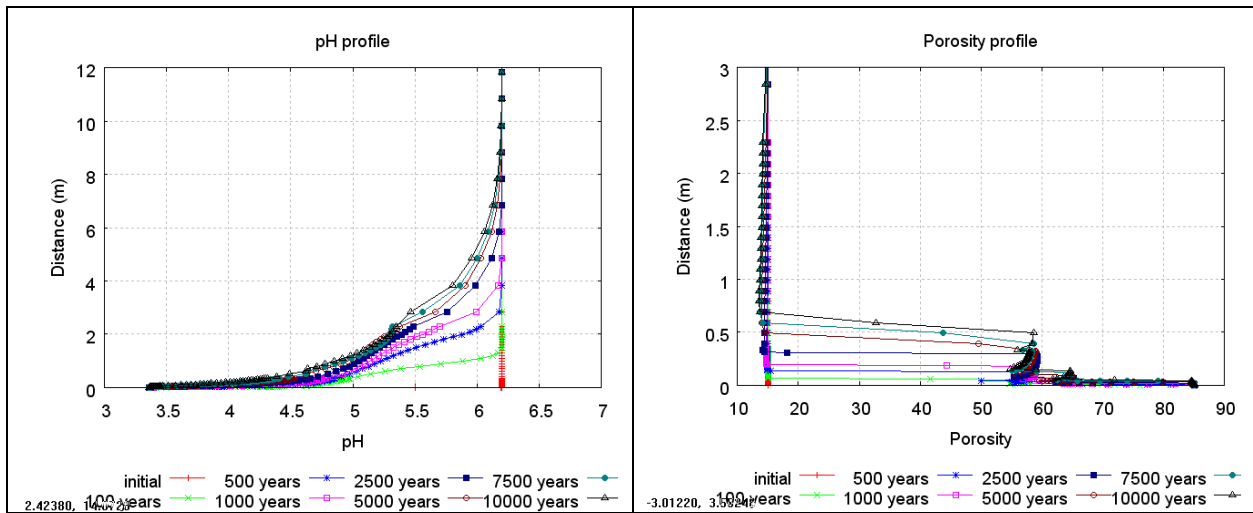
379 observed directly at the reservoir-caprock interface (down to 8% porosity in the first
 380 centimeter). Illite (-11%), calcite (-6%), and montmorillonite (-2%) dissolution is also
 381 observed at this location. Calcite dissolution and anhydrite precipitation occurs only in this
 382 first zone, and a very narrow zone where the montmorillonite remains stable explains the
 383 modest change in porosity (+1%) over a few centimeters. A third zone where clay minerals
 384 (illite and montmorillonite) are destabilized but with precipitation of kaolinite, K-feldspar,
 385 and quartz results in a slight decrease of porosity (1 to 2%). The paragenesis is slightly
 386 different from *case 1a*, especially concerning the behavior of calcite and anhydrite. In *case 1b*,
 387 calcite dissolves and anhydrite precipitates in the sulfate-rich caprock water. These
 388 differences arise from slightly different hypotheses concerning the initial water compositions:
 389 a complete set of minerals is used in *case 1a* (Table 3) vs. “fast reacting” minerals only in
 390 *case 1b* (Table 5). In both cases, however, the impact on the porosity profile remains
 391 comparable.
 392
 393



394

395 **Figure 4. Porosity and pH profiles in the caprock in the case with buffering capacity of the**
 396 **reservoir (pH 4.6). Note the difference of zooming in distance.**

397
 398 The calculations concerning the scenario with the most aggressive water entering the
 399 caprock show a significant alteration of the caprock at the interface, in comparison to the
 400 previous case, with a concomitant increase in porosity (Figure 5). The dissolution of
 401 carbonate (calcite and dolomite) and clay minerals (illite and montmorillonite) is responsible
 402 for the increase of porosity from the initial 15% to an average value of 85% in the first
 403 centimeters directly at the interface, even though kaolinite, anhydrite, and quartz precipitate at
 404 this location. A second front of porosity increase (to almost 60%) reaches 50 centimeters into
 405 the caprock and corresponds to the front of dissolution of carbonates only (calcite and
 406 dolomite). The same minerals as in the first front area also precipitate in this zone, except for
 407 anhydrite which shows a dissolution, up to 15 centimeters, and then a precipitation pattern.
 408 Porosity and pH variations are closely correlated in these calculations.
 409



410

411 **Figure 5. Porosity and pH profiles in the caprock in the case without buffering capacity of the**
 412 **reservoir (pH 3.4). Note the difference of zooming in distance.**

413

414

415

416

417

418

419

420

421

422

423

424

425

426

427

428

429

430

431

432

433

434

435

436

437

438

439

440

441

442

443

444

445

The results show that in this diffusive case, the caprock alteration can be significant and the impact on porosity greatly depends on the water composition and, in particular, on the pH of the solution. In the case of aggressive water with low pH, all the primary minerals are strongly destabilized directly at the interface between the reservoir and the caprock. A significant increase of porosity is also further predicted but the extent remains limited to 50 centimeters: this sharp porosity front corresponds to the complete dissolution of carbonate minerals (calcite and dolomite) where the other primary minerals are rather preserved, resulting in a porosity increase of about 45%. In the interval between these two fronts, mineral adjustments occur leading to an overall “Z-shaped” porosity profile: dissolution of illite and montmorillonite; precipitation of kaolinite and quartz.

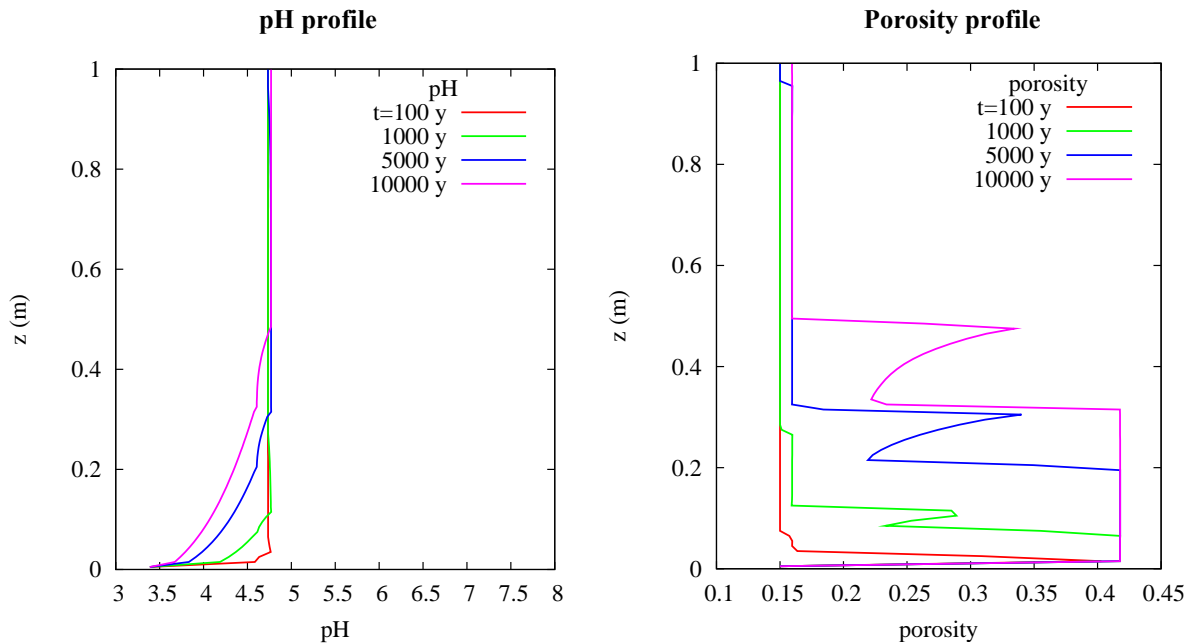
This scenario represents an extreme case where no minerals in the reservoir act as buffer of the pH perturbation, and exemplify the role of the pH of the water at the interface between the reservoir and the caprock. Note also that the mechanical strains that would accommodate at least part of this porosity increase are not taken into account in these calculations. In the other case, the behavior of the system would tend to a slight decrease of the porosity (1%) affecting 3 meters of the caprock. Consequently, if the SC-CO₂ stays confined in the reservoir, the impact of the acidic perturbation on the overall confinement function of a caprock, with a couple of decimeters thickness, will be very low.

435 ***Case 1c: diffusion/slow advection, same initial water composition in reservoir and caprock***

A slightly degraded version of the previous diffusive scenario was simulated. This scenario integrates the effect of a small overpressure in the reservoir compared to the overlying aquifers. This overpressure can result from the injection itself or from the regional hydrological conditions. However, the scenario considers that the overpressure remains low enough so as not to enable a capillary breakthrough of the SC-CO₂: as a result, only dissolved CO₂ (along with the chemical background of the reservoir pore water) can migrate advectively into the caprock.

An upwards 5 mm/y flow was simulated; this would correspond to a 1 m/m hydraulic head gradient with $1.6 \cdot 10^{-18} \text{ m}^2$ permeability, a large upper value for the permeability of a deep argillaceous caprock (e.g. Hildenbrand and Kroos, 2003). The diffusive simulations

446 from *case 1b* (low pH) are reproduced, integrating this slow advection. In particular, the sharp
 447 fronts and the overall "Z-shaped" behavior in the porosity profile are predicted, even though
 448 they slightly differ in amplitude (maximal increase is 30%). Identical reaction pathways are
 449 identified, with reaction fronts progressing slightly faster than in the diffusive case. However,
 450 the progression of the fronts remains limited to the close vicinity of the reservoir/caprock
 451 interface: Figure 6 shows a migration limited to 0.5 m after 10000 y.
 452
 453
 454



455
 456

457 **Figure 6. Advection/dispersion of CO₂-rich solution into the caprock: pH and porosity profile as**
 458 **a function of time.**

459

460 The diffusive-advective scenario simulations show that the migration of dissolved CO₂
 461 remains confined to the first few decimeters of the caprock after hundreds of years under
 462 normal hydrological assumptions: homogeneous caprock, quasi natural regional hydraulic
 463 gradients between the aquifers, no capillary breakthrough.
 464

464

465 ***Conclusion on the diffusive case***

466 As a general conclusion to the calculations in homogeneous diffusive/advective
 467 conditions, we can consider that this case allows us to define a useful reference case for a
 468 better interpretation of the potential impact of the acidified water diffusion along the caprock.
 469 Under the assumptions and the initial and boundary conditions considered here, the impact of
 470 the diffusion of dissolved CO₂ in the caprock is very limited in vertical extension (first
 471 decimeters to meters after 10,000 yrs). The amplitude depends essentially on the pH of the
 472 water in the reservoir at the interface with the caprock (a 45% increase in porosity in the first
 473 50 centimeters in the adverse case of low pH for the reservoir water). In these scenarios, the
 474 long term consequences of the CO₂ perturbation on the caprock integrity thus appear to be
 475 small, especially in the context carbonate-dominant storage systems.
 476

477 The same conclusions are reached by other authors in the literature with slightly
 478 different reactive pathways and consequences on porosity, due to the differences in the initial
 479 mineralogy. In particular, the presence of plagioclase minerals that tend to dissolve,
 eventually leads to the precipitation of minerals such as dawsonite (Gauss et al., 2005;

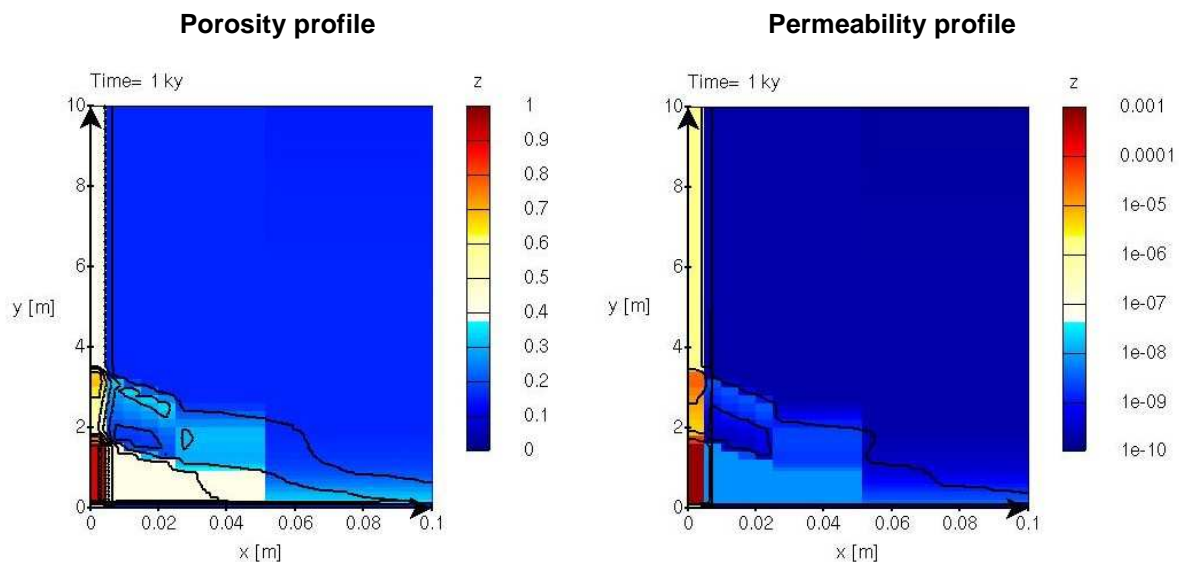
480 Gherardi et al., 2007). The intensity of the reactions and porosity changes (up to 10%, with
 481 comparable increasing and decreasing patterns) modeled by these authors are similar to those
 482 observed in this work, even though the temperature was lower ($\sim 40^\circ\text{C}$).
 483
 484
 485

486 5.2.2. Caprock with discrete fracture

487 *Case 2: diffusive/advective transport in discrete fracture*

488 To investigate the effect of local heterogeneities in the caprock, the advective scenario
 489 (*case 1c*) was degraded with the presence of a discrete fracture. The simulation was translated
 490 into vertical 2D, with an explicit fractured zone: a 5 mm wide half-fracture is created into a
 491 homogeneous caprock, on a 10 m high simulation. A 0.1 m/m hydraulic gradient was given,
 492 with a $1.6 \cdot 10^{-18} \text{ m}^2$ permeability in the bulk matrix, and a permeability 10^4 times higher in the
 493 fractured zone (corresponding to 5 mm/y upflow rate). The chemistry in the matrix is taken
 494 identical to that of the previous reference simulations (*case 1c*); the fractured zone is
 495 considered filled up with calcite, with a remaining porosity of 0.4. These conditions constitute
 496 upper values for a realistic system, in agreement with the safety assessment rules of the
 497 exercise.
 498

499 The simulation results (Figure 7) show a degradation front in the bulk matrix far from
 500 the fracture, in agreement with the previous homogeneous simulations in terms of amplitude.
 501 Closer to the fracture, the locally enhanced flow brings more reacting CO_2 vertically into the
 502 system, so that the reaction front is accelerated (both vertically and horizontally). Inside the
 503 matrix itself, the reaction front is even faster, with a positive feedback of the dissolution of the
 504 calcite, which additionally enhances the fluid flow with the increased permeability in the
 505 reacted area (increased by a factor 10^3).
 506
 507
 508



509
 510 **Figure 7. Distribution of porosity (left) and permeability (right, in m/s) after 1000 years of**
 511 **interactions between the caprock and dissolved CO_2 . The discrete half-fracture is located at the**
 512 **left side of the domain ($x < 5 \text{ mm}$).**
 513

514 The acceleration of the degradation is noticeable in the matrix close to the fracture: 1.5 m
 515 vertically at 1000 y (compared to a 0.4 m/10,000 y in the homogeneous *case 1c*) and in the
 516 fracture itself (4 m after 1,000 years). This is very dependant on the fracture properties:
 517 geometry (aperture), initial permeability, and initial carbonated filling.

518 This is potentially damaging for the sealing properties of the caprock, as opened fractures
 519 could create preferential pathways for SC-CO₂ due to lower local capillary entry pressure. As
 520 a consequence, the reactivity of the carbonated fracture sealing could be furthermore
 521 enhanced, and the reaction front in the fracture even faster.

522 This scenario is different from those already investigated in the literature focusing on the
 523 geochemical effects induced by the advancement of both a CO_{2(aq)}-rich aqueous phase and a
 524 free SC-CO₂ gas plume through a highly porous fractured caprock not filled in by secondary
 525 calcite (Gherardi et al., 2007). Under these conditions, the primary mineralogy of the caprock
 526 is predicted to be altered over the entire length of the fracture.

527

528 Generally speaking, the high reactivity of carbonated minerals, which can occur very soon in
 529 the life of the storage (as opposed to kinetically controlled clay mineral reactivity), raises a
 530 potential risk for the caprock integrity, particularly where these mineral phases are dominant
 531 such as in pre-existing fractures. If it appears that CO₂-saturated water, or SC-CO₂ can
 532 migrate through the caprock, and depending on the transport properties in the fractures, they
 533 could transport the acidic disturbance and potentially open critical pathways for CO₂.

534

535 **5.3. Unsaturated caprock: geochemical interactions with SC-CO₂**

536

537 These calculations correspond to the scenarios where the SC-CO₂ plume make its way
 538 through the caprock either by overcoming the capillary entry pressure of by migration through
 539 an heterogeneity in the caprock (e.g., by mechanical and/or geochemical reactivation of a
 540 discrete fracture or a network of small cracks).

541

542 **5.3.1. Homogeneous caprock and constant capillary properties**

543

544 *Case 3:* In this section, we will consider the presence of CO₂ as a separate gas phase under
 545 supercritical thermodynamical conditions according to the considered temperature and
 546 pressure of 80°C and 150 bar, respectively. The simulations have been conducted using the
 547 reactive transport code TOUGHREACT. In the following, the term “gas phase” actually
 548 refers to SC-CO₂.

549 In this work, a shale thickness of 10 m is simulated and we focus on the geochemical impact
 550 of a possible capillary breakthrough of the gas phase in the caprock. Also, later in this work,
 551 we adjust the model of capillary pressure to alter the capillary entry pressure to allow the
 552 breakthrough capillary (see Appendix for a detailed explanation on the role of entry pressure
 553 on capillary trapping). It is important to note that this study does not deal with the estimation
 554 of the capillary entry pressure of the caprock overlying the Dogger in the Paris Basin
 555 geological context and we refer the reader to Chiquet et al. (2007) for a detailed study on this
 556 topic.

557

558

559 *Relative permeability and capillary pressure model*

560

561 In the framework of the Paris Basin, previous works have been performed to measure
 562 relative permeability and capillary pressure of the so-called Lavoux Limestone considered as
 a good analogue for the Dogger reservoir envisaged as a target for geological storage in

563 France (Lombard, 2008, personal communication). In the following, we will assume similar
 564 trend for relative permeability and capillary pressure model although the cap rock and the
 565 reservoir pore structure may differ from one geological formation to another. Nevertheless,
 566 intrinsic permeability and porosity are chosen in agreement with the expected rock texture
 567 with values of 10^{-13}m^2 and 10^{-18}m^2 assigned to the reservoir and the caprock, respectively.
 568 André *et al.* (2007) have simulated the measured data using the following models:

$$569 \quad K_{rl} = (S^*)^{0.5} (1 - (1 - (S^*)^{1/m})^m)^2 \quad (1)$$

570 with $S^* = (S_l - S_{lr}) / (1 - S_{lr})$; while the gas relative permeability data have been approximated by
 571 the following fourth degree polynomial function:

$$572 \quad K_{rg} = 1.3978 - 3.7694S_l + 12.709S_l^2 - 20.642S_l^3 + 10.309S_l^4 \quad (2)$$

573 with K_{rl} and K_{rg} the corresponding liquid and gaseous relative permeability phase, S_l the
 574 liquid phase saturation, $S_{lr} = 0.2$ the residual liquid phase saturation and $m = 0.6$ the van
 575 Genuchten exponent used in TOUGH2 (see Pruess, 1991). Capillary pressure is approximated
 576 also with a van Genuchten model described by:

$$577 \quad P_{cap} = -P_o ((S^{**})^{-1/m} - 1)^{1-m} \quad (3)$$

578 with P_{cap} the capillary pressure, $S^{**} = (S_l - S_{lr}) / (S_{ls} - S_{lr})$, and P_o a pressure coefficient which
 579 controls the magnitude of the capillary pressure model. In our simulations, we chose
 580 $S_{ls} = 1.05$, $m = 0.6$ and $P_o = 100$ kPa to fit with the data of the Lavoux limestone and to allow
 581 the gas to enter the caprock (see Annexe). Intrinsic permeability values of 10^{-13}m^2 and 10^{-18}m^2
 582 are assigned to the reservoir and the caprock, respectively.

583 *Mesh and boundary conditions*

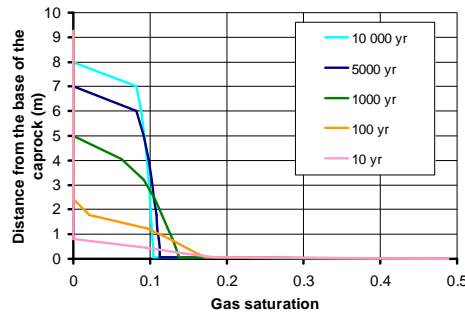
584 The mesh geometry is taken similar to that of the study performed by Xu *et al.* (2005)
 585 to assess the integrity of a caprock composed with minerals of Texas Gulf Coast sediments.
 586 The geometry is 1D cartesian along the vertical direction with a 1 m^2 basal area, and 20 m
 587 long. The reservoir is represented as a unique cell, 10 m long, while the caprock is meshed
 588 with 17 cells progressively increasing in thickness from the reservoir-caprock interface to the
 589 top of the domain (from 0.05 to 1.00 m). The initial state of the system is a hydrostatic profile
 590 of pressure with uniform temperature at 80 C° . A constant pressure boundary was assigned to
 591 the top limit of the domain.

592 In order to assess the presence of CO_2 as a separate gas phase and compare this impact
 593 with the previous simulation, we kept the same initial mineralogical assemblage (Table 3) as
 594 well as a similar initial brine composition in the caprock (Table 2). On the other hand, the
 595 reservoir brine is acidified by adding a gas saturation value arbitrarily chosen to be 0.5. The
 596 CO_2 is assumed to remain in contact with the brine used as a reference (Table 2, column 1)
 597 composition before injection with an initial pressure of 150 bar.

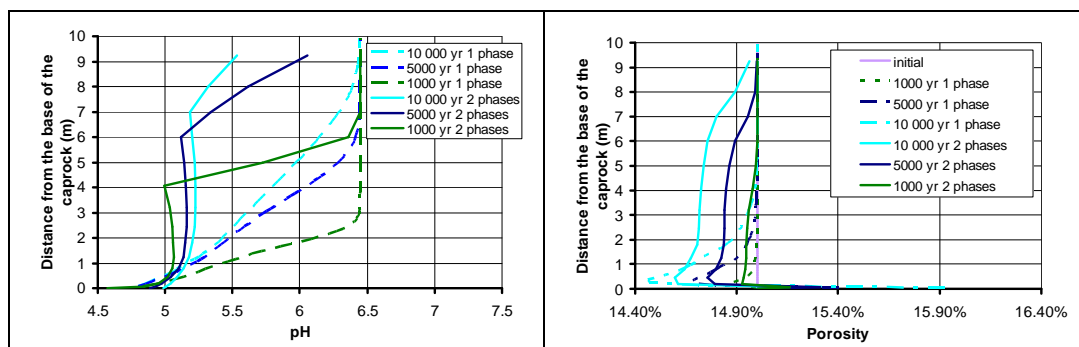
600 *Simulation Results*

601 Figure 8 shows the simulated upward migration of the gas saturation front through the
 602 caprock. After ten years the CO_2 plume has penetrated one meter into the caprock, at 1000
 603 years it reaches 5 m, and at 10 000 years gas has entered about 8 m into the caprock. This
 604 upward migration is controlled by both the capillary entry pressure and the intrinsic
 605 permeability of the caprock. The main process of migration is due to buoyancy effect. Indeed,
 606 at 80 C° and 150 bar, gas and brine density are equal to 430 and 1020 kg/m^3 , respectively. The

613 pH calculated for the reservoir system equals 4.7 (Figure 9), in good agreement with the
 614 homologous single phase simulation scenario previously presented (*Case 1a*). The gas front is
 615 preceded by the dissolution of the gas phase in the brine which acidifies the system. As an
 616 indication, the results of the single-phase and 2-phase simulations are compared in Figure 9.
 617



618
 619 **Figure 8. Gas saturation profiles in the caprock at 10, 100, 1000 and 10 000 years**
 620



621
 622 **Figure 9. pH and porosity profiles at 1000, 5000 and 10 000 years. Comparison with the single**
 623 **phase case**

624
 625 After 10 000 years, the simulations predict a small porosity change similar, in
 626 amplitude, to that observed for the single phase case (*case 1a*) but with a larger extent (Figure
 627 9). This porosity variation is controlled by the mineral dissolution and precipitation processes
 628 which are comparable to that of the single phase scenario. Therefore, considering SC-CO₂ in
 629 the simulation scenario is crucial for the estimate of the capillary trapping in the caprock
 630 which is controlled by the capillary entry pressure and the thickness of the reservoir. On the
 631 other hand, if SC-CO₂ penetrates in the caprock, the induced geochemical alteration of the
 632 shale formation does not differ much from the purely diffusive case prediction, but the
 633 affected region will occupy a larger extent controlled by the gas plume geometry.

634 Other authors in the literature reached the same conclusions with slightly different
 635 reactive pathways and consequences on porosity, again due to the presence of plagioclase
 636 minerals and the precipitation of minerals such as dawsonite (Xu et al., 2005). In contrast, in
 637 some cases (Johnson et al., 2004; Gherardi et al., 2007), and depending on variable conditions
 638 of gas saturation and initial mineralogy, major variations in porosity have been predicted in
 639 the caprock in association with relevant precipitation of other carbonate minerals such as
 640 magnesite and calcite.
 641

642 **6. DISCUSSION**

643
 644 The results of the modeling show that the injection of CO₂ can potentially have a
 645 significant effect on the caprock by changing the mineralogy and changing the porosity due to
 646 the dissolution and precipitation of minerals. Although these changes will in turn induced
 647 changes in the transport properties of the caprock, the impact is limited to a zone ranging
 648 from several decimeters to several meters into the caprock close to the interface with the
 649 reservoir depending on whether the SC-CO₂ plume enters into the caprock and/or if fractures
 650 are present at this location (Table 6).
 651

	pH		Porosity	
	Minimal value	Impact distance into caprock	Absolute change (- clogging, + opening)	Impact distance into caprock
Saturated homogeneous caprock				
Case 1a (with pH perturbation)	4,8	8 m	- 0.2% + 1.8 %	0.5 - 1.5 m 0.1 - 0.2 m
Case 1a (without pH perturbation)	6,2	7 m	+ 2.2 %	0.1 - 0.2 m
Case 1b (pH 4.6)	4,6	8 m	- 7% - 1%	0.01 m 2.5 m
Case 1b (pH 3.4)	3,4	8 m	+ 70% + 40%	0.05 m 0.5 m
Case 1c (diffusion-advection)	3,4	0.5 m	+ 27% + 18%	0.35 m 0.5 m
Saturated fractured caprock				
Case 2 (1000 y)			+ 25%	1.5 m (vertical) 0.05 m (horizontal)
Unsaturated caprock				
Case 3	4,8	10+ m	- 0.5% + 1 %	0.5 - 6 m 0.1 - 0.2 m

652
 653
 654 **Table 6. Overview of minimal pH value and porosity changes with the perturbation distance**
 655 **according to the different scenarios (after 10 000 years or otherwise mentioned in the table).**

656 *Heterogeneities in caprock composition and properties*

657 The presence of fractures with a different composition and set of transport properties
 658 is crucial for the extension of the perturbation. The results obtained with the fracture in the
 659 case 2 show the potential role of other types of heterogeneity, such as the intrinsic
 660 heterogeneity of mineralogical composition or the presence of a network of small cracks in
 661 the caprock. The geochemical behavior in these systems is intricately coupled with the
 662 behavior of the CO₂ plume, through the heterogeneity of capillary properties as demonstrated
 663 for instance by Saadatpoor et al. (2009).
 664

665 The difference between the reactivity of carbonates and clay minerals is the key to the
 666 evolution of the system: short term and short distance for carbonates, long term and long
 667 distance for the clay minerals (see case 1b and case 3). To this regard, one cannot exclude the
 668 role of clay transformations such as the illitisation of smectite or illite/smectite interstratified
 669 minerals, which is observed in experiments (Crédoz et al., 2010) and potentially represents a
 670 further change of properties for the caprock (porosity, permeability, wettability).

671
672 *Conditions for gas entry into the caprock*

673 In a series of scoping hydraulic/geomechanical calculations (Rohmer and Seyedi, 2009),
674 the maximal capillary pressure calculated for an industrial-scale injection of CO₂ into a deep
675 saline aquifer (1 Mt CO₂/yr) is less than 2 bar at the reservoir-caprock interface, far below the
676 capillary entry pressure of most caprocks (see results from WP2, Carles et al. 2009; and
677 Talandier et al. 2006). These results imply that in the conditions of the calculations, the SC-
678 CO₂ plume would not enter into the caprock in the case of a caprock with homogeneous
679 properties. This conclusion has to be reassessed in the case where heterogeneities in the
680 caprock mineral composition could affect the local properties of the rock (such as the
681 capillary curve or relative permeabilities). Also, for injection periods of 10 to 100 years,
682 induced plume entry can be triggered by chemical alteration modifying the pore sizes and
683 structure in the caprock: this scenario was investigated during the project but the model is still
684 under development and shows numerical instability. The pH changes due to the presence of
685 CO₂ can also potentially modify the mineral wettability, although this is still a controversial
686 matter (see e.g. Chiquet et al., 2007; Shah et al. 2008; Fleury et al, *this issue*).

687 During injection, the total overpressure is significant only at the vertical of the injection
688 point ($\Delta P = 35$ bar in Rohmer and Seyedi, 2009) after 10 years of injection and drops to a few
689 bar after the injection stops. These results tend to discard any direct mechanical effect such as
690 fracturing in the caprock during and after the injection phase. Nevertheless, coupled
691 mechanical and chemical processes, such as evidenced here, are maximal in the case of long
692 periods of injection (10 to 100 years) because this would be the typical timescale for
693 carbonate chemical alteration. This phase may turn out to be critical especially with respect to
694 the alteration of the sealing properties of the caprock (Bemer and Lombard, 2009).

695
696 *Consequences of gas entry into the caprock*

697 The results of the calculations with the complete mineralogical and geochemical system
698 predict no significant differences between the case with or without gas entry into the caprock
699 in terms of amplitude of the porosity variations. However, differences are observed on the
700 extent of the impacted zone within the caprock: several meters in the “gas entry” cases
701 whereas it is limited to the first decimeters near the reservoir-caprock interface in the cases
702 without gas entry.

703 704 705 **7. CONCLUSION**

706
707 The results of the modeling of safety scenarios show that in the normal reference case
708 (homogeneous rock, diffusion of dissolved CO₂ only) the impact of the reactivity with CO₂-
709 rich fluids with the carbonate minerals potentially induces significant changes of porosity.
710 Nevertheless, this reactivity is limited to the first decimeters of the caprock close to the
711 interface with the reservoir in 10 000 years and does not lead to any leak from the storage
712 system.

713 Calculations in “degraded” scenarios show that the migration of the perturbation due to
714 SC-CO₂ can extend to several meters within the same period of 10 000 years. These scenarios
715 involve either an alteration of the petrophysical properties of the rock due to the reactivity
716 with CO₂-rich solutions (potentially enhancing small existing heterogeneities) or the
717 reactivation of small cracks or fractures (especially if they are filled with calcite). In both
718 cases, preferential pathways are created for the migration of CO₂ and positive feedback is
719 involved, i.e. more migration leads to more reactivity and more alteration of the transport

720 properties. In these scenarios, any convective component occurring as a result of the alteration
 721 will renew and feed the acid perturbation at critical locations (e.g. richer in carbonates
 722 minerals), and can in turn extend the migration distance of CO₂. One of the key points for the
 723 safety assessment calculations remains the role of these heterogeneities on the behavior of the
 724 storage system. We observe in this work the great influence of structural heterogeneities. The
 725 quantitative assessment of such an impact on the global safety remains an important challenge.
 726

727 To complete a safety assessment for a specific site, a set of conservative (penalizing)
 728 parameters should be adopted for adverse scenarios (such as in *case 1b*) to evaluate the
 729 quantity of CO₂ release from the storage system and the probability of occurrence of these
 730 scenarios should be evaluated from data available from this site (Bildstein *et al.* 2009). The
 731 challenge for the future will be to structure and apply the safety assessment methodology with
 732 an operational finality, in order to support the transition step to carbon geological storage
 733 projects at the industrial scale.
 734

735 8. ACKNOWLEDGEMENTS

736 The authors acknowledge funding from the ANR (the French National Science
 737 Foundation) in the framework of the “Géocarbonate” projects (Injectivité, Carbonation,
 738 PICOREF, CRISCO2) and fruitful discussion with the other partners in these projects. This
 739 project also benefited greatly from the scientific exchanges taking place in the working group
 740 “Modeling at the site scale” animated by E. Brosse (IFP).
 741

742 9. APPENDIX: ROLE OF ENTRY PRESSURE ON CAPILLARY TRAPPING

743 Figure 10 shows the pressure fields of water and carbon dioxide in a geological
 744 storage in aquifer located at a depth H underneath the surface. Once injected, CO₂ occupies
 745 the reservoir pore space available initially filled with water. Due to gravity effects, the storage
 746 area, containing both CO₂ and residual water, is located at the top of the aquifer and has a
 747 thickness h . Point **A** is located at the interface between reservoir and caprock and is part of the
 748 caprock domain. Point **A'** is also located at the interface between reservoir and caprock but
 749 belongs to the reservoir domain. Point **B** is located at the gas-water contact. At this interface
 750 the capillary equilibrium is reached and the capillary pressure is zero. In other words in **B**:
 751

$$752 P_{B,CO_2} = P_{B,H_2O}$$

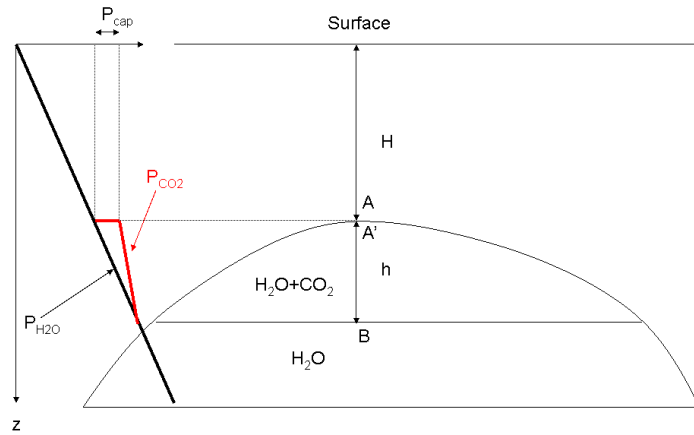
754 In **A**, the water pressure is equal to the water column in the caprock:

$$756 P_{A,H_2O} = \rho_{H_2O} g H$$

758 In **A'**, the CO₂ pressure P_{A',CO_2} is equal to:

$$760 P_{A',CO_2} = P_{A,H_2O} + P_{cap}$$

762 with P_{cap} , the capillary pressure defined as the difference between gas pressure and water
 763 pressure.
 764



765
766 **Figure 10 : CO₂ and H₂O pressure evolution with depth in aquifer storage**

767
768 In the context of geological storage, we define the capillary entry pressure as a
769 capillary pressure threshold representing the resistance of porous network saturated with
770 water to the penetration of carbon dioxide. The capillary entry pressure P_{ce} is intrinsic to the
771 nature of the pore network constituting the clay caprock. According to the Laplace law, it can
772 be expressed as:

$$773 \quad P_{ce} \sim 2\sigma \cos(\phi) / R,$$

774
775 with σ the inter-facial tension between the liquid and gas, ϕ the angle reflecting the ability of
776 the liquid to spread over a surface by wettability, and R the radius of the largest pores
777 (Chiquet et al 2007).
778

779
780 The capillary entry pressure is the value of capillary pressure for a zero gas saturation
781 (Figure 11). The van Genuchten model used in the code Toughreact adjusts the capillary entry
782 pressure using the liquid parameter saturation S_{ls} . For $S_{ls} > 1$, the model of capillary pressure
783 becomes non zero for $S_g = 0$ (Figure 11).
784

785 If the capillary pressure at the caprock-reservoir interface exceeds the capillary entry
786 pressure ($P_{cap-interface} > P_{ce}$), then the CO₂ can penetrate the caprock.
787

788 The capillary pressure in the reservoir-caprock interface $P_{cap-interface}$ is expressed as:

$$789 \quad P_{cap-interface} = P_{A',CO_2} - P_{A,H_2O}$$

790
791 Assuming no change with depth in both CO₂ and H₂O densities, we can write:

$$792 \quad P_{A',CO_2} = P_B - \rho_{CO_2}gh$$

$$793 \quad P_{A,H_2O} = \rho_{H_2O}gH$$

794
795
796
797 On the other hand, considering that:
798
799

800
801
802
803
804
805
806
807
808
809

$$P_B = \rho_{H_2O} g (H+h)$$

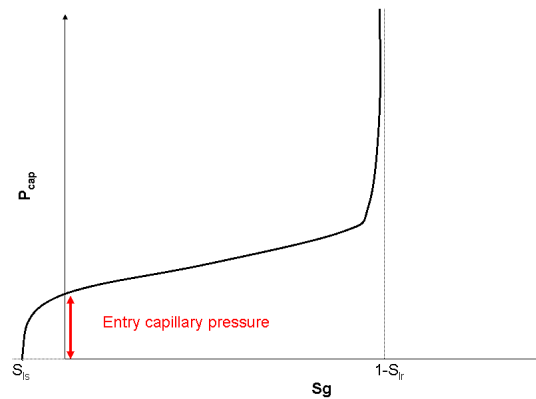
We finally obtain:

$$P_{cap-interface} = (\rho_{H_2O} - \rho_{CO_2}) g h$$

This corresponds to the buoyancy effect induced by density difference between liquid and gas.

Thus, for the gas phase to penetrate the caprock, we must verify that:

$$P_{ce} < (\rho_{CO_2} - \rho_{H_2O}) g h$$



810
811
812
813
814
815
816
817
818
819
820

Figure 11 : Representation of the entry capillary pressure using the van Genuchten model as described in the code TOUGHREACT

In our system, we assume a 10 m thickness for the reservoir. At 150 bar and 80°C, the density of CO₂ is about 430 kg/m³, while the density of water is 1018 kg/m³, which leads for a 10 m thick reservoir to a value of $P_{cap-interface}$ of 57 kPa (0.57 bar). Using a value of $P_o = 100$ kPa in Eq(3) yields a P_{ce} of 54 kPa slightly below $P_{cap-interface}$ and then allowing CO₂ to penetrate the caprock.

821 10. REFERENCES

822
823
824
825
826
827
828
829
830
831
832
833
834
835

- André L., Audigane. P., Azaroual. M., Menjöz. A. (2007) Numerical modelling of fluid-rock interactions at the supercritical CO₂-liquid interface during carbon dioxide injection into a carbonate reservoir, the Dogger Aquifer (Paris basin, France), *Energy Conversion and Management* **48**, 1782-1797
- Azaroual M., Fouillac C., Matray J.M. (1997) Solubility of silica polymorphs in electrolyte solutions, II. Activity of aqueous silica and solid silica polymorphs in deep solutions from the sedimentary Paris Basin, *Chemical Geology* **140**, 167-179.
- Bemer E., Lombard J.M. (2009) From injectivity to integrity studies of CO₂ geological storage: impact of low permeability levels on the experimental investigation of chemical alteration effects on rock petrophysical and geomechanical properties, *Oil Gas Sci. Tech.*, this issue.
- Berne Ph., P. Bachaud, M. Fleury (2009) Diffusion properties of carbonated caprocks from the Paris Basin, *Oil Gas Sci. Tech.*, this issue.

- 836 Bildstein O., Jullien M., Crédoz A., Garnier J. (2009) Integrated modeling and experimental
837 approach for caprock integrity, risk analysis, and long term safety assessment,
838 Proceedings of the GHGT-9 conference, Washington DC, *Energy Procedia* **1**, 3237-
839 3244.
- 840 Carles P., P. Bachaud, E. Lasseur, P. Berne, P. Bretonnier (2009) Confining properties of
841 carbonaceous Dogger caprocks (Parisian Basin) for CO₂ storage purposes, *Oil Gas Sci.*
842 *Tech.*, this issue.
- 843 Chiquet P., Broseta D., Thibeau S (2007) Wettability alteration of caprock minerals by carbon
844 dioxide, *Geofluids* **7**, 112–122.
- 845 Crédoz A., Bildstein O., Jullien M., Géniaut G., Lillo M., Pétronin J.C., Pozo C., Raynal J.,
846 Trotignon L., Pokrovsky O. (2009) Experimental and modeling study of geochemical
847 reactivity between clay minerals and CO₂ in geological conditions, proceedings of
848 GHGT-9 conference, Washington DC., *Energy Procedia* **1**, 3445-3452.
- 849 Crédoz A., Bildstein O., Jullien M., Raynal J., Trotignon L., Pokrovsky O. (2010) Mixed-
850 layer illite-smectite reactivity in co₂-bearing solution: implications for clayey caprock
851 stability in co₂ geological storage, *Appl. Clay Sci.*, *submitted*
- 852 Duan Z., Sun R. (2003) An improved model calculating CO₂ solubility in pure water and
853 aqueous NaCl solutions from 273 to 533 K and from 0 to 2000 bar, *Chemical Geology*
854 **193**, 257– 271
- 855 Fleury M., Berne P., Bachaud P. (2009) Diffusion of dissolved CO₂ in caprock, Proceedings
856 of the GHGT-9 conference, Washington DC, *Energy Procedia* **1**, 2009.
- 857 Fleury M., Kervévan, C., Bildstein, O., Lagneau, T. Pichery, S. Fillacier, M. Lescanne (2009).
858 Géocarbonate-Intégrité program, *Oil & Gas Sci. Tech.*, this issue.
- 859 Gauss I., Azaroual M., Czernichowski-Lauriol I. (2005) Reactive transport modelling of the
860 impact of CO₂ injection on the clayey cap rock at Sleipner (North Sea), *Chemical*
861 *Geology* **217**, 319– 337
- 862 Gauss I., Audigane P, André L., Lions J., Jacquemet N., Durst P., Czernichowski-Lauriol I.,
863 Azaroual M. (2008) Geochemical and solute transport modelling for CO₂ storage, what
864 to expect from it? *Int. J. Greenhouse Gas Cont.* **2**, 605-625
- 865 Gherardi F., Xu T., Pruess K. (2007) Numerical modeling of self-limiting and self-enhancing
866 caprock alteration induced by CO₂ storage in a depleted gas reservoir, *Chemical*
867 *Geology* **244**, 103–129
- 868 Hildenbrand A., Kroos B.M. (2003) CO₂ migration processes in argillaceous rocks: pressure-
869 driven volume flow and diffusion. *Journal of Geochemical Exploration* **78-79**, 169–172.
- 870 Hubert G. (2009), Réactivité expérimentale au CO₂ de roches d'une couverture argileuse et
871 d'un réservoir carbonaté du bassin de Paris. Experimental reactivity with CO₂ of clayey
872 caprock and carbonate reservoir of the Paris basin. PhD Thesis, INPL, Nancy, France,
873 370 p.
- 874 IPCC (2005) IPCC Special Report on Carbon Dioxide Capture and Storage. Prepared by
875 Working Group III of the Intergovernmental Panel on Climate Change [Metz, B., O.
876 Davidson, H. C. de Coninck, M. Loos, and L. A. Meyer (eds.)]. Cambridge University
877 Press, Cambridge, United Kingdom and New York, NY, USA, 442 pp.
- 878 IPCC (2007) Climate Change 2007: Synthesis Report. Contribution of Working Groups I, II
879 and III to the Fourth Assessment. Report of the Intergovernmental Panel on Climate
880 Change [Core Writing Team, Pachauri, R.K and Reisinger, A. (eds.)]. IPCC, Geneva,
881 Switzerland, 104 pp.
- 882 Johnson J.W., Nitao, J.J., Knauss, K.G. (2004) Reactive transport modeling of CO₂ storage in
883 saline aquifers to elucidate fundamental processes, trapping mechanisms, and
884 sequestration partitioning. In: Baines, S.J., Worden, R.H. (Eds.), *Geologic Storage of*
885 *Carbon Dioxide. Geol. Soc. London Spec. Pub.* **233**, 107–128.

- 886 Johnson J.W., Nitao, J.J., Morris, J.P. (2005) Reactive transport modeling of cap rock
887 integrity during natural and engineered CO₂ storage. In: Thomas, D.C., Benson, S.M.
888 (Eds.), *Carbon Dioxide Capture for Storage in Deep Geologic Formations*, vol. 2, 787–
889 813.
- 890 Kohler E., Parra T. (2007) Clayey cap-rock behavior in H₂O-CO₂ media at low pressure and
891 temperature conditions : an experimental approach, 44th Annual Meeting of the Clay
892 Minerals Society, June 2-7, Santa Fe, USA
- 893 Le Gallo Y., Trenty L., Lagneau V., Audigane P., Bildstein O., Mugler C. & E., Mouche
894 (2007) Recent development for long term modeling of CO₂ storage. *In* First French-
895 German Symposium on Geological Storage of CO₂ (Ed A. C. Geotechnologies), GfZ
896 Potsdam.
- 897 Mathias S.A., Hardisty P.E., Trudell M.R., Zimmerman R.W. (2009) Screening and selection
898 of sites for CO₂ sequestration based on pressure buildup, *Int. J. Greenhouse Gas Cont.*
899 **3**(5), 577-585
- 900 Mavko G., Nur A. (1997) The effect of a percolation threshold in the Koseny-Carman relation,
901 *Geophysics* **62**(5), 1480-1482.
- 902 Palandri J., Kharaka Y.K (2004). A compilation of rate parameters of water-mineral
903 interaction kinetics for application to geochemical modelling. US Geological Survey
904 Open File Report 2004-1068
- 905 Parkhurst D.L., Appelo C.A.J., (1999) - User's guide to PHREEQC (Version 2)--A computer
906 program for speciation, batch-reaction, one-dimensional transport, and inverse
907 geochemical calculations: U.S. Geological Survey Water-Resources Investigations
908 Report 99-4259, 312 p.
- 909 Parkhurst D.L., Kipp K.L., Engesgaard P., Charlton S.R. (2004) – PHAST, a program for
910 simulating ground-water flow, solute transport, and multicomponent geochemical
911 reactions. U.S. Geological Survey Techniques and Methods 6-A8, 154 p.
- 912 Pruess, K., 1991, TOUGH2 – a general-purpose numerical simulator for multiphase fluid and
913 heat flow: Lawrence Berkeley Laboratory Report LBL-29400, Berkeley, California
- 914 Rohmer J., D. Seyedi (2009) Addressing caprock failure tendency in deep saline aquifers
915 through large scale hydromechanical analysis: Application to the CO₂ geological
916 storage in the Paris basin case, *Oil Gas Sci. Tech*, this issue.
- 917 Saadatpoor E., Bryant S.L., Sepehrnoori K. (2009) Effect of capillary heterogeneity on
918 buoyant plumes: A new local trapping mechanism, proceedings of GHGT-9 conference,
919 Washington DC., *Energy Procedia* **1**, 3299-3306.
- 920 Shah V., Broseta D., Mouronval G. (2008) Capillary alteration of caprocks by acid gases, SPE
921 113353-PP, Improved Oil Recovery Symposium, Tulsa, OK, USA, 19-23 April 2008.
- 922 Steefel C.I. (2001) CRUNCH: Software for modeling multicomponent, multidimensional
923 reactive transport. User's Guide, UCRL-MA-143182. Livermore, California.
- 924 Talandier J., Mayer G., Croisé J. (2006) Simulations of the hydrogen migration out of
925 Intermediate-level radioactive waste disposal drifts using tough2, Proceedings TOUGH
926 Symposium, Lawrence Berkeley National Laboratory, Berkeley, California
- 927 van der Lee J., L. De Windt, V. Lagneau, and P. Goblet (2003) « Module-oriented modeling
928 of reactive transport with HYTEC », *Computers and Geosciences* **29**, 265-275
- 929 Wolery T.J., (1992). EQ3NR, a Computer Program for Geochemical Aqueous Speciation-
930 Solubility Calculations: Theoretical Manual, Users Guide, and Related Documentation
931 (Version 7.0). Lawrence Livermore National Lab. Report UCRL-MA-110662 PT IV.
- 932 Xu T., Pruess, K. (2001), Modeling multiphase non-isothermal fluid flow and reactive
933 geochemical transport in variably saturated fractured rocks: 1. Methodology: *American*
934 *Journal of Science* **301**, 16-33.

935 Xu T., Apps, J., Pruess, K. (2005), Mineral sequestration of a sandstone-shale system:
936 *Chemical Geology* **217**(3-4), 295-318.
937
938